Brilliance
Research of Artificial Intelligence

E-ISSN : 2807-9035
Volume 4, **Number** 1, May 2024
https://doi.org/10.47709/brilliance.v4i1.3514

The role of the number of transparent covers in enhancing the efficiency of flat plate collectors

Khaled A. Amer[1*], Rahma S. Elzer[2], Ali R. Alkhazmi[3]
[1,3]Department of Mechanical and Renewable Energy, Faculty of Engineering, Wadi Alshatti University, Libya,
[2]Department of physics, Faculty of Science, Derna university, Libya
[1]k.amer@wau.edu.ly, [2]rahmaelzer454@gmail.com, [3]al.alkhazmi@wau.edu.ly

open access

***Corresponding Author**

Article History:
Submitted: 26-01-2024
Accepted: 28-01-2024
Published: 26-02-2024

Keywords:
solar collector; optical efficiency; thermal efficiency; over all heat transfer coefficient; mass flow rate; inlet temperature; transparent cover. Libya

ABSTRACT

Solar energy has gained traction as an eco-friendly alternative to combat Carbon dioxide (CO2) emissions from fired-fossil fuel electrical power plants. One common application is converting solar energy into heat for water heating systems, often achieved through flat-plate solar heating collectors. The useful thermal energy of these collectors depends on factors like climate, design, and operational parameters. This study examines the effect of number of transparent covers (TCs) and the inlet water temperature on the performance of a liquid-flat plate solar collector (LFPSC) in Beida city, Libya, on July 21, 2020, with data collected at hourly intervals. Different scenarios were considered, varying the number of covers (ranging from 0 to 3) and the inlet water temperatures (ranging from 25°C to 50°C). The findings reveal that the optimal number of covers is influenced by multiple factors, not solely the prevailing climatic conditions. Inlet water temperature and the collector's length were identified as the most influential parameters affecting the overall performance of LFPSC. Consequently, the decision to employ a specific number of covers depends on the system's operating conditions. When the inlet water temperature matches the ambient temperature, a single cover suffices for optimal collector performance. However, if the inlet water temperature surpasses the ambient temperature, multiple covers are necessary to achieve the collector's peak efficiency. This research underscores the importance of considering various factors, beyond just climate, when designing and operating solar collectors for efficient water heating systems.

INTRODUCTION

Growing apprehensions regarding environmental issues, such as global warming and climate change, which pose significant threats to both human existence and global ecosystems, have intensified. These challenges are fundamentally driven by the emission of CO_2, predominantly stemming from the fossil fuels burning for electricity and heat production. Notably, electric power stations emerge as the most substantial source of pollution, contributing a substantial 35% of Libya's total CO_2 emissions (Nassar, et al., 2017; Nassar, et al., 2018; Nassar, et al., 2021; Makhzom, et al., 2023).

In a global context, numerous nations have unveiled strategic aspirations to transition toward renewable energy generation, as demonstrated during the COP27 Climate Conference held in Sharm Elsheikh - Egypt from 6 to 18 November 2022, in alignment with the Paris Climate Change Treaty. Libya, a member of the IPCC and a nation that has ratified all pertinent climate change treaties and conventions, has articulated an ambitious objective to augment the role of renewable energies within its electrical energy mix. By the year 2030, Libya aims to attain a 30% share of renewable energy, with this figure poised to escalate to around 55% by 2050. The predominant contributors to this transition will be Photovoltaic and thermal solar energy, and wind energy (Bakouri, et al., 2023; Nassar, et al., 2023).

Libya, centrally located in North Africa, occupies an expanse of 1.8 million square kilometers and boasts an estimated population of 6.735 million. It lies within the "solar belt" experiencing an annual global horizontal solar radiation of approximately 2300 kWh/m^2, equivalent direct solar radiation, and a remarkable 3500 hours of sunlight annually (Yasser, et al., 2023). Fig. 1 visually illustrates the average annual global horizontal irradiation in Libya (https://solargis.com/maps-and-gis-data/download/libya).

Within Libya, the housing sector consumes a significant 36% of the country's total electricity production, with an appreciable 30% dedicated to water heating, constituting roughly 11% of Libya's total electricity generation, as elucidated in Fig. 2 (Alkhazmi & Hamdan, 2023; Abdunnabi, et al., 2018; Tawil, et al., 2018). Consequently, the utilization of solar thermal systems for water heating, boasting an efficiency coefficient of 80%, holds the potential to yield substantial energy savings, amounting to 511,617 MWh/year (Eteriki, et al., 2023). This, in turn, mitigates the release of a substantial volume of carbon dioxide (CO2) into the atmosphere, estimated at approximately 503.15 tons of

Brilliance
Research of Artificial Intelligence

E-ISSN : 2807-9035
Volume 4, **Number** 1, May 2024
https://doi.org/10.47709/brilliance.v4i1.3514

CO_2 per annum. Furthermore, it leads to savings of 148.87 tons of diesel oil and an economic value of $37,736 per year, stemming from the reduction of environmental damage resulting from CO_2 emissions (Nassar, et al., 2023; Makhzom, et al., 2023). Several studies underscore the feasibility and potential of solar heating systems in Libya, highlighting their pivotal role in enhancing energy demand management and facilitating the transition to cleaner energy in the foreseeable future (Algareu, et al., 2021; Tawil, et al., 2019; Abdunnabi, et al., 2016; Abdunnabi, et al., 2017; Abdunnabi, et al., 2019; Abdunnabi & Musa, 2021; Saed, et al., 2017; Almabrouk & Abulifa, 2023; Andeef, et al., 2023; Nassar, 2015).

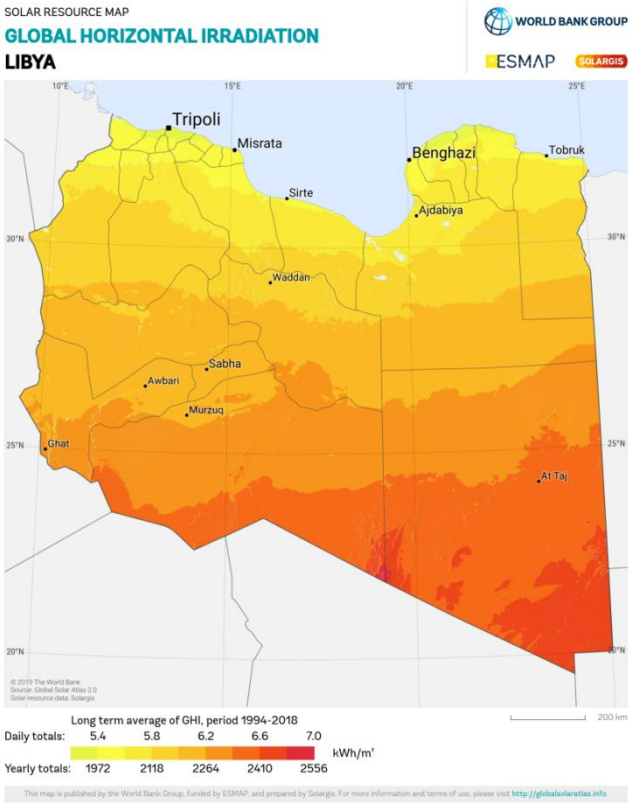

Figure 1. Annual average global irradiation in Libya

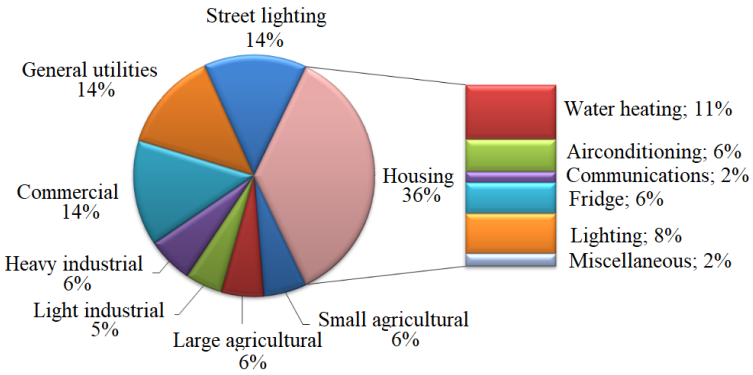

Figure 2. Breakdown of electricity consumption in Libya

LITERATURE REVIEW

Solar collectors serve as the cornerstone in thermal engineering systems. Fig. 3 provides a detailed representation of a domestic solar hot water supply system (Yasser, et al., 2023). LFPSCs typically comprise three primary components: an absorber plate for intercepting and converting solar energy into useful energy for the working fluid, a transparent cover allowing solar rays to pass while reducing top heat loss, and a layer of insulation on the reverse side to reduce bottom heat loss (Nassar, 2006). The efficiency of a solar collector depends on how solar radiation, incident on its surface, is reflected, transmitted, and absorbed by TCs and the absorber plate. These optical properties, encompassing transmissivity, reflectivity, absorptivity, and emissivity, are influenced by parameters like thickness (l),

Brilliance
Research of Artificial Intelligence

E-ISSN : 2807-9035
Volume 4, **Number** 1, May 2024
https://doi.org/10.47709/brilliance.v4i1.3514

refraction index (n), and extinction coefficient (k), all of which are functions of light wavelength and incident solar angle (Nassar, 2006).

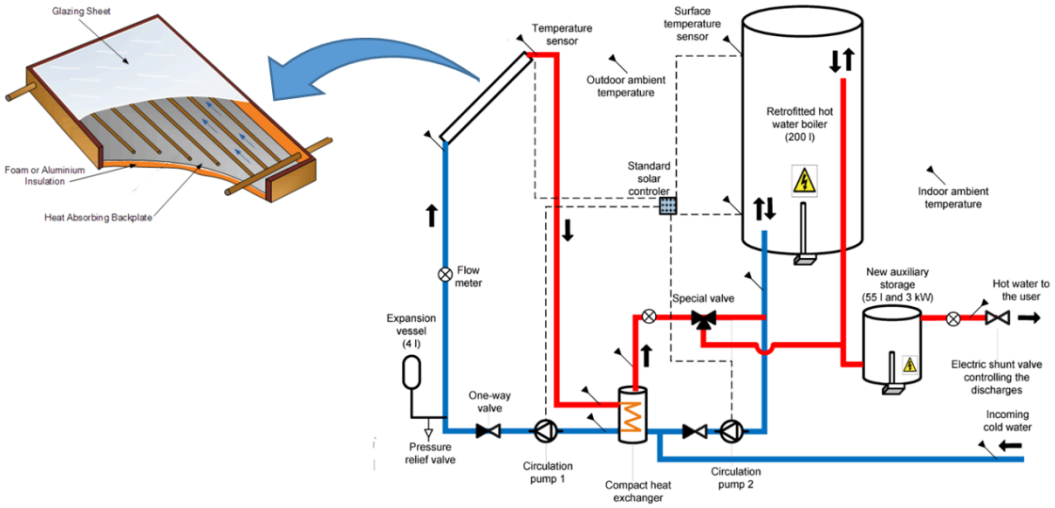

Figure 3. A schematic diagram of water heating solar flat-plate collector

Glass stands out as an appealing material for solar collectors due to its high transmissivity, long-term stability, environmental friendliness, and cost-effectiveness. Spectroscopically selective coatings, reflecting infrared light, can be applied to the glass surface, further reducing heat losses (Nassar, 2006). Number of TCs, (n) and (l) will significantly affect the solar collector's performance. Hence, it becomes imperative to determine the optimal number of covers and an effective refractive index, enabling enhanced efficiency, irrespective of solar insolation levels and geographical location (Giovannetti, 2014).

Researchers like Kalidasan and Srinivas conducted investigations into the impact of the number of TCs and n on LFPSCs performance. Their study simulated the performance of a LFPSC at VIT University Vellore, considering different numbers of TCs (ranging from 0 to 3) and various n values (ranging from 1.1 to 1.7). The outcomes revealed that the collector's efficiency increased with the addition of more covers up to a certain optimum point, after which it began to decrease. Furthermore, efficiency decreased with higher refractive index values (Kalidasan & Srinivas, 2014). In a similar vein, Bakari et al. explored the effects of (l) on LFPSC performance, employing low iron (extra clear) glass with thicknesses of 3, 4, 5, and 6 mm. Their findings indicated that the collector with 4 mm thick glass demonstrated the highest efficiency (Bakari, et al., 2014). Supriti's research delved into the influence of the number of TCs and (n) on the performance of a domestic solar hot water supply system. The results underscored that increasing the number of TCs improved the LFPSC's efficiency. However, efficiency declined with higher refractive index values. The most significant useful heat gain was observed when using 3 TCs with an (n) value of 1.1 (Supriti, 2015). Vettrivel and Mathiazhagan conducted a comparative study on single and double glazings for LFPSCs. Their findings revealed that double glazing exhibited higher efficiency compared to single glazing under the same condition (Vettrivel & Mathiazhagan, 2017). Chabane and Sekseff conducted an experimental study on a double glazing air heater solar collector in Biskra - Algeria. Experimental results highlighted that minimizing forward thermal losses significantly improved the solar collector's performance, and the addition of a second glass layer effectively reduced these losses in a solar air collector (Chabane & Sekseff, 2018).

In light of existing literature, it becomes evident that there is a research gap concerning the determination of the optimal number of TCs, (n), and (l), all of which can potentially enhance the performance of LFPSCs. Most research efforts have primarily concentrated on the properties of glass cover materials. Consequently, this paper centers its focus on identifying the optimum number of TCs and their corresponding (n) values, with the ultimate goal of boosting the performance of solar flat plate collectors.

METHOD

The overall efficiency of an LFPSC is the product of its optical efficiency by its thermal efficiency. These last two have been assessed under various scenarios, encompassing single, double and triple covers. For each cover configuration, the optical, thermal and then overall efficiencies have been computed while accounting for different (*n*) values, specifically 1.1, 1.4, and 1.7. These calculations were conducted over the course of a single day, specifically July 21st, from 8 a.m. to 4 p.m., with readings taken at hourly intervals. The performance evaluation was based on the specifications and dimensions outlined for the LFPSC, as detailed in Table 1 (Bakari, 2014).

Brilliance
Research of Artificial Intelligence

E-ISSN : 2807-9035
Volume 4, **Number** 1, May 2024
https://doi.org/10.47709/brilliance.v4i1.3514

Table 1. Specification of LFPSC

Metric	Value
Collector type	Liquid flat plate
Solar collector dimension (Length × Width)	3.105 m × 1.219 m
Absorber plate dimension (Length × Width)	2.975 m × 1.168 m
Spacing bewteen TC and absorber plate	0.024 m
Spacing between TCs	0.024 m
Thermal conductivity of the absorber plate	401 W/mK
Thickness of TC	0.203 mm
Absorptivity of the absorber plate	0.93
Outer diameter of lateral tube	0.0127 m
Inner diameter of lateral tube	0.0114 m
Tube center to center distance	0.0115 m
Bottom loss coefficient	0.08 W/m2°C
Cover extinction coefficient	4 m-1
Water flow rate	0.05 kg/s
Inlet water temperature	Parameter (Tamb, 30, 40, 50°C)
Ambient temperature	Variable
Wind speed	3 m/s
Collector's side loss coefficient	Negligible
Collector's inclination angle	11°, south facing
Date	July 21st, December 21st
Location	Beida, Libya (32.76 oN,21.75 oE)

Study site information

Beida city is nestled in northeastern Libya, atop the picturesque Green Mountain, precisely located at 32°45′59″N latitude, 21°44′30″E longitude and 623 m above sea level. Beida observes the UTC+2 time zone (Eastern European Time - EET). Beida experiences distinct seasons throughout the year. The warm season spans approximately 4.6 months, commencing from May 23 and stretching until October 9. During this period, the city enjoys an average daily high temperature exceeding 26°C. The hottest month of the year is August, with an average high of 28°C and a low of 19°C. Conversely, the cool season encompasses about 3.2 months, starting from December 5 and concluding on March 12. Throughout this season, the average daily high temperature remains below 16°C. The coldest month is January, with an average low of 6°C and a high of 13°C. Beida witnesses a rainy season lasting for 6.1 months, from October 5 to April 8, during which consistent rainfall is observed, with a sliding 31-day average of at least 12.7mm. January stands out as the wettest month, with an average rainfall of 45.7 mm. The windier part of the year unfolds over 4.9 months, spanning from November 21 to April 16, characterized by average wind speeds exceeding 5.32 m/s. February holds the title of the windiest month, with an average hourly wind speed of 6.13 m/s. The predominant wind direction is from the north for 6.7 months, prevailing from April 21 to November 11, with a peak percentage of 81% on July 25. From November 11 to April 21, the prevailing wind direction is from the west, with a peak percentage of 42% on January 1. The sunniest period of the year extends for 3.6 months, starting on May 6 and ending on August 26, during which the city basks in an average daily global horizontal solar radiation exceeding 7.3 kWh/m2. July is the brightest month, boasting an average of 8.3 kWh/m2. Daylight hours in Beida vary throughout the year. The earliest sunrise occurs at 5:24 AM on June 12, while the latest sunrise is at 7:36 AM on January 9. The earliest sunset takes place at 5:26 PM on December 4, and the latest sunset occurs at 7:45 PM on June 30. The year can be divided into two distinct sky conditions. The clearer part spans approximately 4.0 months, commencing around June 3 and concluding around October 2, with July being the clearest month. On the other hand, the cloudier part of the year persists for approximately 8.0 months, commencing around October 2 and concluding around June 3. December emerges as the cloudiest month, during which the sky is overcast or mostly cloudy about 34% of the time (Alsadi & Yasser, 2016). For a visual representation of Beida's location, wind speed, air temperature, and global horizontal solar irradiance, please refer to Figure 4.

Brilliance
Research of Artificial Intelligence

E-ISSN : 2807-9035
Volume 4, **Number** 1, May 2024
https://doi.org/10.47709/brilliance.v4i1.3514

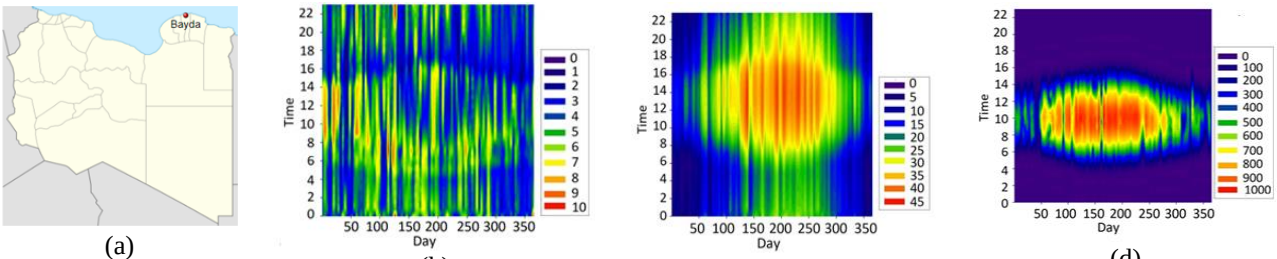

Figure 4. Beida city location (a), Wind speed (b), Air Temperature (c), and Global horizontal solar irradiance (d).

Approach's assumptions

To conduct a thorough and comprehensive investigation, it becomes necessary to introduce certain assumptions. These assumptions serve the purpose of simplifying the analysis and preventing the need for excessively costly computations:

1. Constant thermal properties;
2. Steady state situation;
3. The solar radiation incident homogenously over all the collector surface;
4. The side heat loss is negligible;
5. No shading on the absorber plate;
6. Each component at a uniform temperature.
7. The upper and lower heat losses from the surfaces of the solar collector are at one dimension.

Research's limitations

As it was later realized that large number of design, climatic and operation parameters affect the optimum design of solar collectors, and each condition has a special optimum design. The main limitations of the study that are, the impact of design and operation parameters are not considered such as solar collector's area, length, tilt angle, mass flow rate, which planned to be future investigations.

Mathematical approach

The formulas below are used to find solar time as the first step in the numerical calculation (Nassar, 2006).

Solar angles

Solar declination angle **(**δ)

$$\delta = 23.45\ sin\left\{\frac{360\ (284+n)}{365}\right\} \quad (1)$$

Where n is the number of days calculated from January 1st.

Hour angle (ω)

$$\omega = 15\ (ST - 12) \quad (2)$$

Where ST is the solar time.

Solar Zenith angle (θ_z)

$$\theta_z = cos^{-1}(sin\emptyset.sin\delta + cos\emptyset.cos\delta.cos\omega) \quad (3)$$

Where $\emptyset$ is the site latitude angle.

Solar incident angle (θ_i) for south facing collector

$$\theta_i = cos^{-1}(sin(\emptyset - \beta).sin\delta + cos(\emptyset - \beta).cos\delta.cos\omega) \quad (4)$$

Where β is the collector inclination angle.

Calculation of global tilted solar irradiance

The global horizontal solar irradiance (I_h) is composed of two components: the direct beam (I_{bh}) and the sky-diffuse (I_{dh}). These components are calculated using the following relationships (Alsadi & Yasser, 2016):

$$I_h = I_{bh} + I_{dh} \quad (5)$$

The calculation of solar irradiance on inclined surfaces (I_t) can be carried out in the following manner (Alsadi & Yasser, 2016):

Brilliance
Research of Artificial Intelligence

E-ISSN : 2807-9035
Volume 4, **Number** 1, May 2024
https://doi.org/10.47709/brilliance.v4i1.3514

$$I_t = I_{bh}R_b + I_{dh}R_d + I_h\,R_r \tag{6}$$

The conversion of direct solar radiation is a straightforward process, often accomplished by utilizing the transportation factor R_b. This factor is contingent on the geometric characteristics of the inclined surface and the sun's position. It is expressed as follows:

$$R_b = max\left(0, \frac{cos\,\theta_i}{cos\,\theta_z}\right) \tag{7}$$

In these equations, θ_i represents the solar incidence angle, θ_z denotes the solar zenith angle, and R_d and R_r stand for the sky diffuse radiation and ground reflected radiation view factors, respectively. In recent years, various authors have introduced transposition models for R_r . However, it's a common practice to make the assumption of isotropic albedo radiation (Alsadi & Yasser, 2016).

$$R_r = \rho_g \frac{1 - \cos\beta}{2} \tag{8}$$

Here, ρ_g represents the ground reflectivity or albedo, which is typically assumed to be 0.2 in many cases (Alsadi & Yasser, 2017). The calculation of sky-diffuse irradiation is carried out using the Bugler Plan of Array transposition model, as outlined in (Nassar, et al., 2022; Abdulwahab, et al., 2023; Nassar et al., 2019; Alsadi, et al., 2016).

$$R_d = \frac{1 + cos\beta}{2} + 0.05\frac{I_{bh}}{I_{dh}}R_b \tag{9}$$

Analysis of the optical properties of a flat-plate solar collector

The transmissivity (τ), reflectivity (ρ), absorbtivity (α) and emissivity (ε) characteristics of a material are determined by its thickness in m (l), reflective index rate (n), and the optical incidence factor in m^{-1} (k). In the model employed for this study, the cover material is glass, with varying refractive indices. The amount of solar flux that reaches the surface of the plate is influenced by the solar incidence angle (θ_1), and this is contingent on the cover's transmissivity. To compute the optical efficiency (η_{opt}), we use (θ_1) as the angle of incidence, which is then incorporated into Snell's law to account for transmissivity, reflection, and absorption (Nassar, 2006).

$$\frac{sin\theta_1}{sin\theta_2} = \frac{n_2}{n_1} \tag{10}$$

Where $\frac{n_2}{n_1}$ represents the refractive index ratio.

$$\rho_1 = \frac{sin^2(\theta_2 - \theta_1)}{sin^2(\theta_2 + \theta_1)} \tag{11}$$

$$\rho_2 = \frac{tan^2(\theta_2 - \theta_1)}{tan^2(\theta_2 + \theta_1)} \tag{12}$$

For a system consisting of M covers, the transmittance can be expressed as follows:

$$\tau_b = \frac{1}{2}\left(\frac{1-\rho_1}{1+(2M-1)\rho_1} + \frac{1-\rho_2}{1+(2M-1)\rho_2}\right) \tag{13}$$

Applying Bouguer's law, the absorption-based transmittance can be calculated as follows:

$$\tau_d = e^{-kd/cos\theta_2} \tag{14}$$

The reflection-refraction and absorption independently can be used to calculate the transmissivity of a collector's cover system, which is determined by the product form.

$$\tau = \tau_b.\tau_d \tag{15}$$

The product of transmissivity and absorptivity (τα) for beam radiation is provided as follows (Nassar, 2006):

$$(\tau\alpha)_b = \frac{\tau\alpha}{1-(1-\alpha)\rho_b} \tag{16}$$

Now, the total solar radiation absorbed by the collector can be calculated as (Nassar, 2006):

$$S = I_b r_b(\tau\alpha)_b + \{I_d r_d + (I_b + I_d)r_r\}(\tau\alpha)_d \tag{17}$$

With the knowledge of the solar radiation incident (I_T) on the top of the glass cover and the solar radiation absorbed by the absorber plate (S), the optical efficiency (η_{opt}) can be expressed as (Nassar, 2006):

$$\eta_{opt} = \frac{S}{I_T} \tag{18}$$

Thermal analysis of LFPSC

To determine both the collector heat removal factor (F_R) and the overall loss coefficient (U_l,), an iterative approach is employed. Given that these two values are interdependent, one is determined with the other assumed to be reasonable. The calculation for the thermal efficiency of the flat plate collector is conducted under this assumption for

Brilliance
Research of Artificial Intelligence

E-ISSN : 2807-9035
Volume 4, **Number** 1, May 2024
https://doi.org/10.47709/brilliance.v4i1.3514

the overall heat loss coefficient (U_l). To find the collector heat removal factor (F_R), the collector efficiency factor (F') is computed from (Nassar, 2006):

$$F' = \frac{1}{WU_l\left[\frac{1}{U_l(D_0 + (W - D_0)F)} + \frac{1}{C_b} + \frac{1}{\pi D_i h_{fi}}\right]} \quad (19)$$

In the given context: F represents the fin's efficiency; W is the spacing between the tubes in m; D_0 and D_i are the outer and inner diameters of the tube in m; U_l is the overall heat loss coefficient in W/m^2K; C_b is the bond's conductance in $W/m\,K$, calculated as $\left[\frac{k_b b}{\gamma}\right]$; where k_b is the bond's thermal conductivity in $W/m\,K$, b is the bond's width in m, and γ is the average bond's thickness in m; h_{fi} is the convection coefficient of the fluid. The fin's efficiency can be determined as (Nassar, 2006):

$$F = \frac{tanh\,[m\,(W - D_o)]/2}{m\,(W - D_0)/2}, \text{ where } m = \sqrt{\frac{U_l}{kd}} \quad (20)$$

Where: k is the thermal conductivity of plate in $W/m\,K$; d is the plate thickness in m. The collector heat removal factor F_R can be expressed as (Nassar, 2006):

$$F_R = \frac{\dot{m}c_p}{A_c U_l}\left[1 - exp\left(-\frac{F' A_c U_l}{\dot{m}c_p}\right)\right] \quad (21)$$

Where: $\dot{m}$ denotes the water flow rate in kg/s ; c_p represents the water specific heat capacity in $J/kg\,K$; A_c stands for the collector area in m^2. The useful energy gain (q_u) can be articulated as follows:

$$q_u = A_c F_R\left[I_T(\tau\alpha) - U_l(T_{fi} - T_a)\right] \quad (22)$$

Where: T_{fi} is the inlet water temperature; T_a signifies the ambient temperature.
The (U_l) is comprised of the coefficients for top, edge, and back losses, as detailed in reference (Nassar, 2006).

$$U_l = U_t + U_e + U_b \quad (23)$$

The top loss coefficient (U_t) is calculated using Klein's empirical formula (Yasser, et al., 2023):

$$U_t = \left\{\frac{N}{\frac{C}{T_{pm}}\left[\frac{T_{pm} - T_a}{N + f}\right]^e} + \frac{1}{h_w}\right\}^{-1} + \frac{\sigma(T_{pm} + T_a)(T_{pm}^{\,2} + T_a^{\,2})}{A + B - N}$$

In equation (24), A, B, f, C, e and hw are presented by the following equations

$$A = \left(\varepsilon_p + 0.00591\,Nh_w\right)^{-1}$$
$$B = \frac{2N + f - 1 + 0.133\,\varepsilon_p}{\varepsilon_g}$$
$$f = (1 + 0.089\,h_w - 0.1166\,h_w\varepsilon_p)(1 + 0.07866\,N) \quad (24)$$
$$c = 520\,(1 - 0.000051\,\beta^2)\;for\;0 < \beta < 70^o.for 70^o < \beta < 90^0 \quad \text{, use } \beta = 70^o$$
$$e = 0.430\left(1 - \frac{100}{T_{pm}}\right)$$

$$h_w = 5.7 + 3.8\,v \quad (25)$$

In the analysis, several parameters come into play: σ represents the Stefan-Boltzmann constant; N stands for the number of TCs; β is the collector inclination angle; ε_g is the glass cover's emissivity; ε_p is the absorber plate's emissivity; v represents the wind speed; h_w is the heat transfer coefficient due to wind. The calculation process involves finding the mean temperature T_{pm}. Initially, an assumed value is used to estimate U_l and q_u. The subsequent T_{pm}values are iteratively calculated using a specific equation, with the initial value being adjusted in each iteration to converge towards the desired result, as outlined in reference (Yasser, et al., 2023):

$$T_{pm} = T_{fi} + \frac{q_u/A_c}{U_l F_R}(1 - F_R) \quad (26)$$

The instantaneous thermal efficiency of the solar collector is given as (Yasser, et al., 2023)

$$\eta = \frac{q_u}{A_c I_T} \quad (27)$$

.

Brilliance
Research of Artificial Intelligence

E-ISSN : 2807-9035
Volume 4, **Number** 1, May 2024
https://doi.org/10.47709/brilliance.v4i1.3514

RESULT

A MATLAB code was developed to simulate how the number of glass covers impacts the thermal performance of the solar collector, with useful energy serving as a reference for the optimization process. Figure 2 illustrates the simulated climate data.

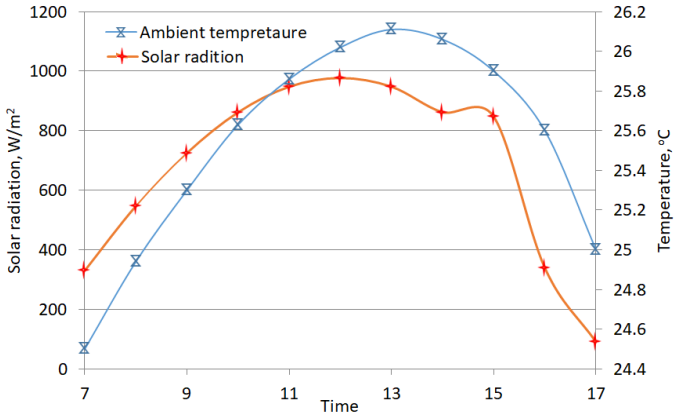

Figure 5. The climatic conditions for July 21st 2021.

Figure 6 illustrates the optical efficiency for the solar collector tilted with an angle of 11°, south facing for the four variants of covers.

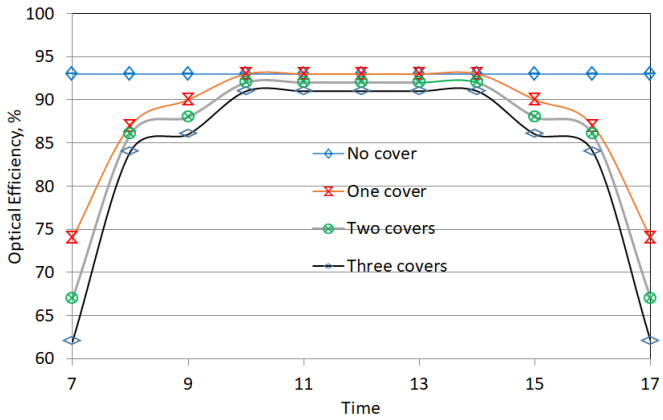

Figure 6. Optical efficiency of the solar collector as a function with the number of covers

Figure 7 provides a representation of the average top loss heat transfer coefficient (Ut) as a function of both the number of covers and the inlet water temperature.

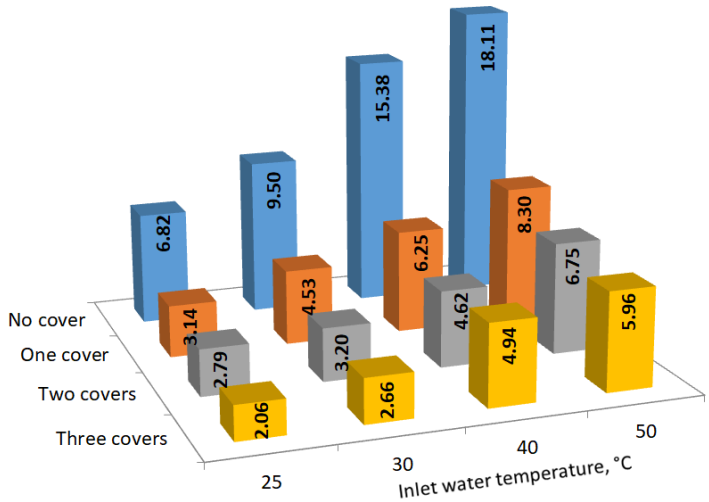

Figure 7. Average top loss heat transfer coefficient U_t W/m^{2}K corresponding to various numbers of cover and inlet water temperatures.

Brilliance
Research of Artificial Intelligence

E-ISSN : 2807-9035
Volume 4, **Number** 1, May 2024
https://doi.org/10.47709/brilliance.v4i1.3514

Figure 8 provides an illustration of the total daily heat gain flux (qu) in W/m² of the solar collector, showcasing its relationship with both the number of covers and the inlet water temperature under the given operational and climatic conditions.

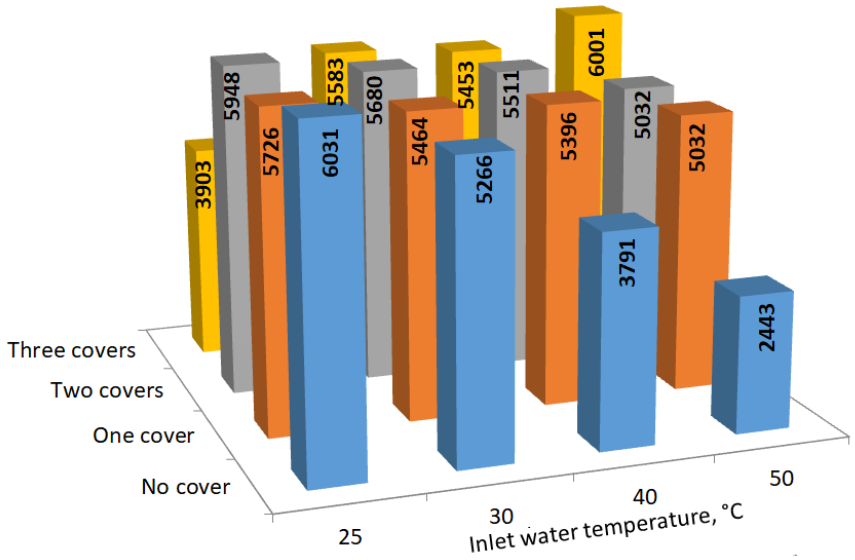

Figure 8. Total daily solar heat gains flux W/m^2 corresponding to various numbers of cover and inlet water temperatures.

DISCUSSION

As depicted in Figure 6, the addition of more covers to the solar collector leads to a decrease in its optical efficiency. Additionally, it's noticeable that the optical efficiency is relatively low in the morning hours but increases around noon, primarily due to the phenomenon of light diffraction resulting from the large incidence angle.

From Figure 7, it's evident that the number of glass covers has a significant effect on reducing the Ut (top loss heat transfer coefficient) of the solar collector, while the water inlet temperature has an inverse effect on Ut. The addition of glass covers increases the thermal resistance between the absorber plate and its surroundings, resulting in a reduction in Ut. On the other hand, the impact of the water inlet temperature is indirect. A higher water entry temperature leads to a higher absorber plate temperature, which, in turn, increases the radiative heat transfer coefficient between the absorber plate and the sky, as demonstrated in (Nassar & Sergievsky, 2000; Yasser, et al., 2019; Yasser, et al., 2023).

The useful energy gain is determined by the subtracting the absorbed solar energy by the absorber plate and the energy lost. In this context, the impact of the inlet water temperature is evident: higher inlet temperatures result in less heat transferred from the absorber plate to the water due to the smaller temperature gradient between the absorber plate and the working fluid. The effect of the number of covers is somewhat complex. On one hand, adding covers to the collector reduces the solar energy that absorbed by the absorber plate. On the other hand, it increases the thermal resistance between the plate and its surroundings, subsequently reducing heat losses. Therefore, finding the optimum design point requires balancing the maximization of absorbed solar radiation with the minimization of heat loss. This balance is influenced by various design factors (such as collector length), operating conditions (such as mass flow rate), and climatic parameters (including solar radiation, ambient temperature, and wind speed). As a result, the conclusions drawn here are specific to the current case and the collector's specifications listed in Table 1. From Figure 8, the following conclusions can be drawn, especially at relatively high flow rates:

- When $T_{fi} < T_a$ (inlet temperature is less than ambient temperature), the heat gain from the surroundings exceeds that from solar energy. In this case, reducing thermal resistance is favourable for the solar collector, making it more suitable to operate without any covers.
- When $T_{fi} = T_a$ (inlet temperature equals ambient temperature), the optimum number of covers is one.
- When $T_{fi} > T_a$ (inlet temperature is greater than ambient temperature), the goal of the solar collector shifts to preserving its energy from being lost and maximizing gains from solar energy. Therefore, increasing the number of covers benefits the thermal performance of the solar collector.

It's important to note that the length of the solar collector is a critical parameter in these results. As the collector length increases, so do the losses. Therefore, apart from economic considerations, selecting the appropriate collector length is essential to achieve the desired temperature under specific flow conditions.

Brilliance
Research of Artificial Intelligence

E-ISSN : 2807-9035
Volume 4, **Number** 1, May 2024
https://doi.org/10.47709/brilliance.v4i1.3514

CONCLUSION

Using MATLAB software, a theoretical analysis was conducted to assess the thermal behavior of water heating flat-plate solar collectors under the specific climatic conditions of Beida city on July 21, 2020. A solar collector with specifications outlined in Table 1 was examined, considering various design and operating parameters, including four different numbers of transparent covers (0, 1, 2, and 3 covers) and four different inlet water temperatures (25, 30, 40, and 50°C) into the solar collector. The results obtained reveal that the optimal number of covers is influenced by multiple factors, and it's not solely determined by climatic conditions, as is often assumed. In particular, the water inlet temperature and the length of the solar collector emerge as the most influential parameters in determining the thermal behavior of the solar collector. Therefore, the decision regarding the number of covers is a mutliobjective problem depends on the function, climatic and operation conditions of the whole system. When the inlet water temperature to the solar collector matches the ambient temperature, one cover is sufficient to achieve optimal performance. However, when the water inlet temperature is higher than the ambient temperature, the use of more than one cover becomes necessary to attain the solar collector's optimum performance.

REFERENCES

Abdunnabi, M., Rohuma, I., Endya, E., & Belal, E. (2018). Review on solar water heating in Libya. *Solar Energy and Sustainable Development Journal*, *7*(SI), 1-27. DOI: 10.51646/jsesd.v7iSI.72

Abdunnabi, M., Dadesh, K., Mrehel, O., & El-shamekh, N. (2016). Effect of full implementation of domestic solar water heaters on the electricity peak load in Libya. *Solar Energy and Sustainable Development Journal*, *5*(2), 33–43. DOI: 10.51646/jsesd.v5i2.62

Abdunnabi, M., Al-Ahjal, M., & Rahoma, I. (2017). Optimum sizing of residential active solar water heating systems for Libyan families. *Solar Energy and Sustainable Development Journal*, *6*(1), 18–26. DOI: 10.51646/jsesd.v6i1.58

Abdunnabi, M., Loveday, D., &. Wright, J. (2019). Development of a design tool for sizing and optimizing thrmosyphon solar water heater systems: a case study for Tripoli-Libya. *Solar Energy and Sustainable Development Journal*, *8*(1), 1–11. DOI: 10.51646/jsesd.v8i1.17

Abdunnabi, M., & Musa, M. (2021). Towards strategic plan for wide spreading of solar water heaters in Libya. *Solar Energy and Sustainable Development Journal*, *2*(1), 12-25. DOI: 10.51646/jsesd.v2i1.93

Abdulwahab, S., Fathi, Y., El-Khozondar, H., Khaleel, M., Ahmed, A., & Alsharif, A. (2023). Meeting solar energy demands: significance of transposition models for solar irradiance. *International Journal of Electrical Engineering and Sustainability (IJEES)*, *1*(3), 90–105.

Algareu, A., Abdunnabi, M., Mabruk, M., & Elmaghrabi, A. (2021). Legionella bacteria activity investigation in domestic water heating systems: Tripoli-Libya as a case study. *Solar Energy and Sustainable Development Journal*, *10*(2), 11–20. DOI: 10.51646/jsesd.v10i2.114

Alkhazmi, A., Hamdan, M. (2023). An experimental and theoretical study of the performance of the thermal storage using phase change materials. *International Journal of Electrical Engineering and Sustainability (IJEES)*, *1*(3), 60–73.

Almabrouk, A., & Abulifa, S. (2023). The technology of renewable energy and its role in achieving sustainable development. *International Journal of Electrical Engineering and Sustainability (IJEES)*, *1*(2), 1–9.

Alsadi, S., & Yasser, N. (2016). Correction of the ASHRAE clear sky model parameters based on solar radiation measurements in the Arabic countries. *International Journal of Renewable Energy Technology Research*, *5*(4), 1-16.

Alsadi, S., & Yasser, N. (2017). Estimation of Solar Irradiance on Solar Fields: An Analytical Approach and Experimental Results. *IEEE Transactions on Sustainable Energy*, *8*(4), 1601-1608. DOI: 10.1109/TSTE.2017.2697913

Alsadi, S., Yasser, N., Amer, K. (2016). General polynomial for optimizing the tilt angle of flat solar energy harvesters based on ASHRAE clear-sky model in mid and high latitudes. *Energy and Power, Scientific& Academic Publishing*, 6(2).

Andeef, M., Bakouri, K., Ahmed, B., Gait, A., El-Batta, F., Foqha, T., & Qarqad, H. (2023). The role of renewable energies in achieving a more secure and stable future. *International Journal of Electrical Engineering and Sustainability (IJEES)*, *1*(2), 11–20.

Bakari, R., Minja, R., & Njau, K. (2014). Effect of glass thickness on performance of flat plate solar collectors for fruits drying. *Journal of energy*, ,p. 1-8

Bakouri, K., Foqha, T., Ahwidi, O., Abubaker, A., Nassar, Y., & El-Khozondar, H. (2023). Learning lessons from Murzuq-Libya meteorological station: Evaluation criteria and improvement recommendations. *Solar Energy and Sustainable Development Journal*, *12*(2), 30-48. DOI: 10.51646/jsesd.v12i1.149

E-ISSN : 2807-9035
Volume 4, **Number** 1, May 2024
https://doi.org/10.47709/brilliance.v4i1.3514

Chabane, F., & Sekseff, E. (2018). Experimental study of a solar air collector with doubles glazed. *Iranian (Iranica) Journal of Energy & Environment*, *9*(3), 163-167.

Elnaggar, M. (2023). Useful energy, economic and reduction of greenhouse gas emissions assessment of solar water heater and solar air heater for heating purposes in Gaza, Palestine. *Heliyon*, 9, e16803.

Eteriki, M., El-Osta, W., Nassar, Y., & El-Khozondar, H. (20223). Effect of implementation of energy efficiency in residential sector in Libya. *The 8th International Engineering Conference on Renewable Energy & Sustainability CRES 2023*, Gaza-Palestine, 2023.

Giovannetti, F. (2014). High transmittance, low emissivity glass covers for flat plate collectors: Applications and performance. *Solar energy*, *30*(4), 106-115.

https://solargis.com/maps-and-gis-data/download/libya

Kalidasan, B., & Srinivas, T. (2014). Study on effect of number of transparent covers and refractive index on performance of solar water heater. *Journal of Renewable Energy*, 1-11.

Makhzom, A., Aissa, K., Alshanokie, A., Yasser, N., El-Khozondar, H., Salem, M., Khaleel, M., Bazina, M., & Elmnifi, M. (2023). Carbon dioxide life cycle assessment of the energy industry sector in Libya: A case study. *International Journal of Electrical Engineering and Sustainability (IJEES)*, *1*(3), 145–163.

Makhzom, A., Eshdok, A., Nassar, Y., Alsadi, S., Foqha, T., Salem, M., AlShareef, I., & El-Khozondar, H. (2023). Estimation of CO2 emission factor for power industry sector in Libya. *The 8th International Engineering Conference on Renewable Energy & Sustainability (ieCRES 2023)*, May 8-9, 2023, Gaza Strip, Palestine. DOI: 10.1109/ieCRES57315.2023.10209528.

Nassar, Y. (2015). Thermodynamics analysis and optimization procedure for domestic solar water heating system. *American Journal of Energy and Power Engineering*, *2*(6), 92-99.

Nassar, Y. (2006). Solar energy engineering active applications, Sabha University, Sebha - Libya.

Nassar, Y., Abuhamoud, N., Miskeen, G., El-Khozondar, H., Alsadi, S., & Ahwidi, O. (2022). Investigating the applicability of horizontal to tilted sky-diffuse solar irradiation transposition models for key Libyan cities. *2022 IEEE 2nd International Maghreb Meeting of the conference on Sciences and Techniques of Automatic control and computer engineering (MI-STA 2022)*, 23-25 May 2022 Sabratha-Libya.

Nassar, Y., Aissa, K., & Alsadi, S. (2018). Air pollution sources in Libya. *Research & Reviews: Journal of Ecology and Environmental Sciences*, *3*(1), 63-79.

Nassar, Y., Aissa, K., & Alsadi, S. (2017). Estimation of environmental damage costs from co2e emissions in Libya and the revenue from carbon tax implementation. *Low Carbon Economic*, *8*(3), 118-132.

Nassar, Y., El-Khozondar, H., Abouqeelah, M., Abubaker, A., Miskeen, A., Khaleel, M., Ahmed, A., Alsharif, A., Elmnifi, M. (2023). Simulating the energy, economic and environmental performance of concentrating solar power technologies using SAM, Libya as a case study. *Solar Energy and Sustainable Development Journal*, 12(2), 1-20. DOI: 10.51646/jsesd.v12i2.153.

Nassar, Y., El- Khozondar, H., Abohamoud, N., Abubaker, A., Ahmed, A., Alsharif, A., & Khaleel, M. (2023). Regression model for optimum solar collectors' tilt angles in Libya. *The 8th International Engineering Conference on Renewable Energy & Sustainability (ieCRES 2023)*, May 8-9, 2023, Gaza Strip, Palestine. DOI: 10.1109/ieCRES57315.2023.10209547.

Nassar, Y., Hafez, A., & Alsadi, S. (2019). Multi-factorial comparison for twenty-four distinct transposition models for inclined surface solar irradiance computation, study case: State of Palestine. *Frontiers in Energy Research*. DOI: 10.3389/fenrg.2019.00163.

Nassar, Y., Salem, M., Iessa, K., AlShareef, I., Amer, K., & Fakher, M. (2021). Estimation of CO2 emission factor for the energy industry sector in Libya: A case study. *Environment, Development and Sustainability*, *23*(1), 13998-14026. doi:10.1007/s10668-021-01248-9.

Nassar, Y., & Sergievsky, E. (2000). Heat transfer in flat-plate solar air-heating collectors. *WIT Transactions on Engineering Sciences*, 10(2), 1-10, DOI:10.2495/HT000531.

Saed, J., Abdunnabi, M., Essnid, A., & Buishi, A. (2017). New designed thermosyphon solar water heater with small sized parabolic trough collectors. *Solar Energy and Sustainable Development Journal*, *6*(2), 30–41. DOI: 10.51646/jsesd.v2i1.93

Supriti, S. (2015). Study to find out the optimum number of transparent covers and refractive index for the best performance of sunearth solar water heater using matlab software, in *Science in Technology*. 2015, Arizona State University: USA.

Tawil, I., Abeid, M., Abraheem, E., Alghoul, S., & Dekam, E. (2018). Review on solar space heating - cooling in Libyan residential buildings. *Solar Energy and Sustainable Development Journal*, 7(SI), 78-112. DOI: 10.51646/jsesd.v7iSI.76

Tawil, I., BenAbeid, M., Belhaj, S., & Sowid, B. (2019). Simulation and evaluation of solar water heating systems availability in mosques sector in the city of Tripoli- Libya. *Solar Energy and Sustainable Development Journal*, *8*(1), 1–17. DOI: 10.51646/jsesd.v8i1.19

E-ISSN : 2807-9035
Volume 4, **Number** 1, May 2024
https://doi.org/10.47709/brilliance.v4i1.3514

Vettrivel, H., & Mathiazhagan, P. (2017). Comparison study of solar flat plate collector with single and double glazing systems. *International Journal of Renewable Energy Research (IJRER)*, *7*(1), 266-274.

Yasser, N., Alatrash, A., Elzer, R., Alkhazmi, A., El-Khozondar, H., Alsharif, A., Ahmed, A., & Khaleel, M. (2024). Optimum Number of Glass Covers of Thermal Flat Plate Solar Collectors. *Wadi Alshatti University Journal of Pure and Applied Sciences*, 2(1), 1-10.

Yasser, N., Alsadi, S., Amer, K., Yousef, A., & Fakher, M. (2019). Numerical analysis and optimization of area contribution of the PV cells in the PV/T flat-plate solar air heating collector. *Solar Energy Research Update*, *6*(2), 43-50.

Yasser, N., Amer, K., El- Khozondar, H., Ahmed, Ab., Alsharif, A., & Khaleel, M. (2023). Thermoelectrical Analysis of a New Hybrid PV/T Flat-Plate Solar Collector. The 8th International Engineering Conference on Renewable Energy & Sustainability (ieCRES 2023), May 8-9, 2023, Gaza Strip, Palestine, pp. 1-5, doi: 10.1109/ieCRES57315.2023.10209472.

Yasser, N., El-Khozondar, H., Ghaboun, G., Khaleel, M., Yusupov, Z., Ahmed, A., & Alsharif, A. (2023). Solar and wind atlas for Libya. *International Journal of Electrical Engineering and Sustainability (IJEES)*, *1*(3), 27-43.

Yasser, N., Elzer, R., Alkhazmi, A., El-Khozondar, H., Essid, M., & Mbaye, A. (2023). Thermal analysis of air-heating flat-plate thermal solar collectors. *International Journal of Electrical Engineering and Sustainability (IJEES)*, *1*(3), 129–144, 2023.